An Improved Method For Real-Time Monitoring of Membrane Capacitance in *Xenopus laevis* Oocytes

Bernhard M. Schmitt and Hermann Koepsell
Department of Anatomy & Cell Biology, University of Würzburg, 97070 Würzburg, Germany

ABSTRACT Measurements of membrane capacitance (C_m) in *Xenopus laevis* oocytes offer unique experimental possibilities but are difficult to perform with current methods. To improve C_m measurements in the two-electrode voltage clamp (TEVC) mode, we developed a paired-ramp protocol and tested its performance in a model circuit (with tunable C_m, membrane resistance R_m, and series resistance R_s) and in *Xenopus* oocytes. In the cell model and with $R_s = 0\ \Omega$, inaccuracy of C_m estimates was <1% under widely varying conditions (R_m ranging from 100 to 2000 kΩ, and C_m from 50 to 1000 nF). With $R_s > 0\ \Omega$, C_m was underestimated by a relative error ϵ closely approximated as $\varepsilon \approx 2 \times R_s/(R_s + R_m)$, in keeping with the theoretical prediction. Thus, ε may be neglected under standard conditions or, under extreme conditions, corrected for if R_s is known. Relative imprecision of C_m estimates was small, independent of R_s, and inversely related to C_m (<1.5% at 50 nF, <0.4% at 200 nF). Averaging allowed reliable detection of C_m deviations from 200 nF of 0.1 nF, i.e., 0.05%. In *Xenopus* oocytes, we could resolve C_m changes that were small (e.g., $\Delta C_m \approx 2$ nF upon 100 μM 8-Br-cAMP), fast (e.g., $\Delta C_m/\Delta t \approx 20$nF/30s upon 1 μM phorbol myristate acetate (PMA)) or extended and complex (e.g., fast increase, followed by prolonged C_m decrease upon 1 μM PMA). Rapidly alternating between paired ramps and a second, step protocol allowed quasi-simultaneous monitoring of additional electrical parameters such as R_m, slope conductance g_m, and reversal potential E_{rev}. Taken together, our method is suited to monitor C_m in *Xenopus* oocytes conveniently, with high temporal resolution, accuracy and precision, and in parallel with other electrical parameters. Thus, it may be useful for the study of endo- and exocytosis and of membrane protein regulation and for electrophysiological high-throughput screening.

INTRODUCTION

The most basic electrical properties of biological membranes are conductance (G_m) and capacitance (C_m). To understand the electrical properties of cells and the functioning of the nervous system, both parameters need to be studied. Historically, it was capacitance that was measured first. In 1923, Fricke applied impedance analysis to various cell suspensions and used his capacitance data to derive the first, remarkably accurate estimate of the thickness of biological membranes (Cole, 1968). Only much later were the first experimental estimates of membrane conductance obtained by extracellular recordings from the squid giant axon (Cole and Hodgkin, 1939).

Soon, the biological relevance of membrane capacitance was realized, e.g., for the propagation of electric impulses in nerve cells, or for synaptic integration. Besides geometry, the decisive parameter herein is the specific capacitance, defined as the capacitance per unit area. The specific capacitance of squid axons was estimated to be ~1.0–1.3 μF/cm^2 (Curtis and Cole, 1938).

Because specific capacitance is rather constant in a given cell (Gentet et al., 2000), it can be taken as a marker of a cell's membrane surface area. Thus, capacitance measurements provided, for instance, great qualitative and quantitative detail about membrane dynamics associated with oocyte maturation and fertilization (for review, see Kado, 1993). When the patch-clamp technique emerged, it was soon applied to study exocytosis via membrane capacitance measurements (Neher and Marty, 1982), next to the analysis of single ion channel currents. C_m measurements using the new technique could subsequently be refined to such a degree that single vesicle fusion events, i.e., capacitance changes smaller than 1 fF on a millisecond time scale, can be resolved (Lindau and Neher, 1988; Gillis, 1995; Chen and Gillis, 2000; Gillis, 2000).

Besides being a read-out of surface area, membrane capacitance can provide valuable information about membrane proteins, by virtue of their complex and specific dielectric properties. For instance, substrate binding to, or conformational changes of, integral membrane proteins involve charge displacements within the electrical field and can turn membranes into highly nonlinear, time-varying capacitors. In this respect, viewing membrane proteins as insulators with specific dielectric properties is no less rewarding than viewing them as conductors. For instance, this approach is used to study the gating of ion channels (Armstrong, 1975; Keynes, 1994) or to map kinetically the transport cycles of membrane transporters (Birnir et al., 1991; Parent et al., 1992; Loo et al., 1993; Klamo et al., 1996; Forster et al., 1998).

Capacitance monitoring can be of particular usefulness in *Xenopus laevis* oocytes. This experimental system has developed into a mainstay of current research because of the ease and flexibility with which heterologous proteins can be

Submitted August 2, 2001, and accepted for publication November 28, 2001.

Address reprint requests to Dr. Bernhard M. Schmitt, Department of Anatomy & Cell Biology, University of Würzburg, Koellikerstrasse 6, 97070 Würzburg, Germany. Tel.: 49-931-3127-05; Fax: 49-931-312087; E-mail: bernhard.schmitt@mail.uni-wuerzburg.de.

0006-3495/02/03/1345/13 $2.00

expressed and characterized functionally via the two-electrode voltage clamp (TEVC) technique. One example for the potential contribution of capacitance measurements in *Xenopus* oocytes is the regulation of ion channels and transporters. To a large extent, this regulation relies on the insertion and retrieval of membrane proteins via endo- and exocytosis, in *Xenopus* oocytes as well as in native tissues (Khan et al., 1991; Blumenthal and Kaczmarek, 1992; Bourinet et al., 1992; Murray et al., 1994; Isom et al., 1995; Hirsch et al., 1996; Klamo et al., 1996; Loo et al., 1996; Takahashi et al., 1996; Quick et al., 1997; Zhu et al., 1997; Forster et al., 1999). Conversely, and similarly exciting, some transport proteins seem to impact on endo-/exocytosis (Piwon et al., 2000). In this context, C_m measurements offer one of the most direct and useful means to assess membrane surface area and its dynamics. Such measurements allow the important distinction between effects on insertion or retrieval on the one hand and direct regulatory effects on protein function on the other (Vasilets et al., 1990; Blumenthal and Kaczmarek, 1992; Hirsch et al., 1996; Klamo et al., 1996; Loo et al., 1996; Takahashi et al., 1996; Mastroberardino et al., 1998; Forster et al., 1999; Weber et al., 1999; Tong et al., 2001).

Furthermore, the *Xenopus* oocyte system lends itself perfectly to study the mechanisms of endo- and exocytosis in general, beyond the specific angle of membrane protein trafficking. In small cells, C_m measurements using patch-clamp techniques have already been applied widely and successfully to study these processes. In *Xenopus* oocytes, numerous additional questions surrounding these processes could be approached by C_m measurements, because the individual components of the endo- and exocytosis machinery can here be manipulated individually and specifically, drawing from a wide repertoire of established strategies (Schmalzing et al., 1995; Quick et al., 1997; Mastroberardino et al., 1998; Peters et al., 1999; Alvarez et al., 1999). Optionally, C_m measurements can be combined in this system with fluorescent, amperometric, or biochemical endo-/exocytosis assays (Angleson and Betz, 1997) or with mechanical stimuli (Zhang and Hamill, 2000).

Somewhat surprisingly, however, C_m measurements have actually been conducted only sporadically in *Xenopus* oocytes, leaving these two promising avenues virtually untraveled. The main reason for this situation seems to be the lack of a powerful yet straightforward method to measure C_m. Admittance measurements using sinusoidal voltage commands and phase-locked amplifiers (Weber et al., 1999; Awayda, 2000), for instance, are too cumbersome and demanding for a more general use. In addition, the effort associated with the TEVC variety of this particular approach is not rewarded by similar low noise and high time resolution as is the case with the patch-clamp counterpart (Weber et al., 1999; Awayda, 2000). Ramp and step protocols, on the other hand, have not been modified substantially since their introduction 30 years ago (Palti, 1969; Adrian and Almers, 1974), thus wasting the opportunity to exploit modern computers and software to improve their performance.

In the present work, we attempted to make C_m measurements in *Xenopus* oocytes better and simpler. To this end, we used a modified voltage ramp stimulus that improved analytical performance by using signal averaging, by omitting the portions of the I_m trace that are susceptible to distortion, and by a design that avoids some problems encountered with other methods, such as dielectric dispersion phenomena (sine-wave stimulation) or deviation of capacitive transients from simple exponential shape (square-wave stimulation). Systematic characterization of method performance in a model circuit and in native oocytes showed that this modified ramp approach is suited to monitor C_m in *Xenopus* oocytes with high accuracy and precision and is robust in the face of high R_s, low R_m, or non-ideal voltage clamp conditions. All other parameters required for the complete electrical characterization of basic biomembranes can be monitored simultaneously with C_m. This straightforward method should facilitate studies of exocytosis, endocytosis, hormonal regulation of membrane transport proteins in *Xenopus* oocytes, and the use of C_m measurements in electrophysiological high-throughput screening.

METHODS

Rationale

Four basic ways to measure C_m can be distinguished, based on the parameters that are used to calculate C_m (for reviews, see Cole, 1968; Kado, 1993; Gillis, 1995). 1) Voltage ramps are employed to elicit constant capacitive currents I_{cap}. Under the assumption that $I_{cap} \approx I_m$, C_m can easily be calculated according to $C_m = I_{cap} \times dt/dV$ (Palti, 1969). With significant noncapacitive current components, a more involved version of this approach becomes necessary (Johnson and Thompson, 1989). 2) Voltage steps are used to elicit a capacitive transient I_{cap}, the integral of which is related to the size of the voltage step ΔV and to capacitance C_m according to $C_m = Q_{cap}/\Delta V$ (Adrian and Almers, 1974; Peres and Bernardini, 1985; Kado, 1993). 3) Voltage steps and the associated capacitive transient may be analyzed in an alternative way. Namely, the measured peak current at $t = 0$ and the fitted time constant τ of the ideally monoexponential current decay allow one to solve for C_m. Analogously, a current step can be used to determine C_m in the current clamp mode (Kado, 1993). 4) Sinusoidal voltage commands are used to probe membrane admittance (or impedance), from which relative C_m changes or absolute C_m values can be computed. Several variants of this approach exist, which may include phase-sensitive detection; single, dual, or multiple frequencies; and various algorithms for the fitting and correction procedures involved (Gillis, 1995).

Among these four basic approaches, we chose voltage ramps as a starting point for our attempt to improve C_m measurements because several lines of evidence and reasoning suggested that their theoretically achievable performance in the particular setting of TEVC measurements in *Xenopus* oocytes should be equal to or better than the performance of the other three approaches (see Discussion). Notably, voltage ramps are also the most straightforward way to measure C_m. In contrast, admittance measurements put considerable demands on hardware, software, and electrophysiology skills of the experimenter, apparently without much room for simplification.

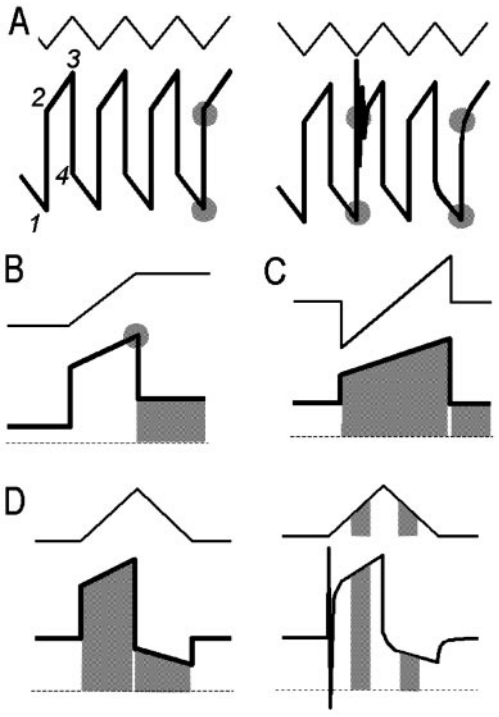

FIGURE 1 Optimizing ramp-shaped voltage stimuli for capacitance measurements. The thin upper traces show command voltage (V_c); thick lower traces show corresponding current response (I_m); single I_m values (*shaded circles*) or I_m integrals (*shaded polygons*): parameters required to determine C_m. (*A*) Continuous symmetrical triangular ramps. The difference 1–3 is easy to determine, but not exact unless R_m approaches infinity (*left side*) (Palti, 1969). The differences 1–2 or 3–4 yield exact values but are difficult to determine under non-ideal clamp conditions (*right side*) (Johnson and Thompson, 1989). (*B*) Simple ramp. Trace portions used for C_m determination are more robust than in *A* and can in part be determined using signal averaging. (*C*) Modified simple ramp. In this particular case, $\int I_{res} - \int I_{hold} = 0$; averaging/integration can be applied to all parameters. (*D*) Paired ramps. As in *C*, averaging/integration can be applied to all parameters. In addition, the C_m determinations from *D* are generally valid, both for linear and nonlinear *I-V* relationships. Time windows in which relevant parameters are measured can be set at a distance from portions that are particularly susceptible to distortion under non-ideal clamp conditions (*right side*).

So far, ramp-based capacitance measurements in whole cells or preparations thereof used sawtooth stimuli, i.e., continuous, triangular ramps (Fig. 1 *A*) (Palti, 1969; Moody and Lansman, 1983; Neher, 1971; Moody and Bosma, 1985; Block and Moody, 1987; Johnson and Thompson, 1989). In its simple version (Palti, 1969; Neher, 1971; Moody and Lansman, 1983; Moody and Bosma, 1985; Block and Moody, 1987), the approach treats the membrane as a pure capacitor, neglecting its conductance. A more exact version (Johnson and Thompson, 1989) requires determining I_m at two particular time points to obtain the capacitive component of I_m (left side of Fig. 1 *A*, shaded circles). This procedure precludes, however, the use of signal averaging within one ramp. Furthermore, one of the points is rather sensitive to non-ideal voltage clamp conditions (right side of Fig. 1 *A*), and cumbersome corrections or approximations may become necessary (Johnson and Thompson, 1989).

Alternatively, a single ramp in conjunction with a segment where V_m is constant, such as shown in Fig. 1 *B*, would allow us to use signal averaging for one of the required parameters and to choose a time window sufficiently far away from the transition from ramp to constant segment. Yet another ramp profile, such as presented in Fig. 1 *C*, would allow us to determine both required parameters through signal averaging, and both time windows for averaging may be set at a distance from the transition points. Finally, the ramp profile shown in Fig. 1 *D* would have the same advantages as the ramp shown in Fig. 1 *C*, i.e., the possibility to use averaging and to avoid the transition zones. In addition, however, this ramp has lesser requirements as to the constraints that must be fulfilled to yield valid C_m estimates and is therefore applicable to a much wider set of electrical networks. In particular, these paired ramps yield exact C_m values even for equivalent circuits with arbitrarily nonlinear, voltage-dependent parallel resistances and current sources (see next paragraph). Therefore, we chose the ramp type shown in Fig. 1 *D* for our attempts to improve C_m measurements by the TEVC technique.

Calculation of C_m

Capacitance is calculated from the charges flowing during two voltage ramps, one depolarizing (or hyperpolarizing) and one repolarizing. From Q_A and Q_B, the current integrals during the two respective ramps, and the known ramp height ΔV, the capacitive charge Q_{cap} associated with ΔV can be separated out algebraically simply as $Q_{cap} = 1/2(Q_A - Q_B)$, and capacitance is calculated as $C_m = Q_{cap}/\Delta V = 1/2(Q_A - Q_B)/\Delta V$.

This approach is illustrated in Fig. 2. It can be applied to passive, linear networks (Fig. 2 *A*) but also to active, nonlinear networks with voltage-dependent elements (Fig. 2 *B*); in either case, however, network properties must be strictly time independent.

Consider first the passive, linear network shown in Fig. 2 *A*, consisting of a resistor R_m and a parallel capacitance C_m. Passivity means that $I_m(0\ mV) = 0$ mA, and linearity means that the differentials dI_m/dV_m and dQ_m/dV_m have constant values, independent of V_m or time. The total current I_m at any time t and voltage V_m is the sum of two components, resistive current (I_{res}) and capacitive current (I_{cap}):

$$I_m = I_{res} + I_{cap} \tag{1}$$

The charge $Q_{res}(A)$ that is moved across R_m by I_{res} during ramp A is given by the corresponding integral of $I_{res}(t)$. Ramp B runs through the same voltage profile, just in opposite direction. For symmetrical ramps, $Q_{res}(B)$ therefore has the same magnitude and sign as $Q_{res}(A)$:

$$Q_{res}(B) = Q_{res}(A) \equiv Q_{res} \tag{2}$$

Asymmetrical ramps with two different slopes may be used as well for C_m determinations, but apart from slightly different algebra there are neither advantages nor disadvantages. For instance, data in Figs. 7 and 8 were acquired using slopes that differed by a factor of 2. In a linear capacitance C_m, the current $I_{cap}(t)$ is $I_{cap} = C_m \times dV/dt$, and the charge associated with ΔV during ramp A is $Q_{cap}(A) = C_m \times \Delta V$. For ramp B, ΔV has an opposite sign:

$$Q_{cap}(B) = -Q_{cap}(A) \tag{3}$$

For simplicity, we define $Q_{cap}(A) \equiv Q_{cap}$. The total charges flowing during each ramp are termed Q_A and Q_B, respectively. We can express Q_A and Q_B as the sums of resistive and capacitive charges: $Q_A = (Q_{res} + Q_{cap})$, and $Q_B = (Q_{res} - Q_{cap})$. The sum of Q_A and Q_B is a pure resistive charge, because the capacitive components are of opposite sign and cancel each other out. It follows that $Q_{res} = (Q_A + Q_B)/2$, and therefore $Q_{cap} = (Q_A - Q_{res}) = 1/2(Q_A - Q_B)$. Finally, capacitance is calculated as follows:

$$C_m = (Q_A - Q_B)/(2\Delta V) \tag{4}$$

Next, consider an active, nonlinear network as the one shown in Fig. 2 *B*. The network is termed active because of the current source; as a formal consequence, the *I-V* and *Q-V* relationships may have nonzero values at $V_m = 0$ mV. Furthermore, the network is termed nonlinear because the

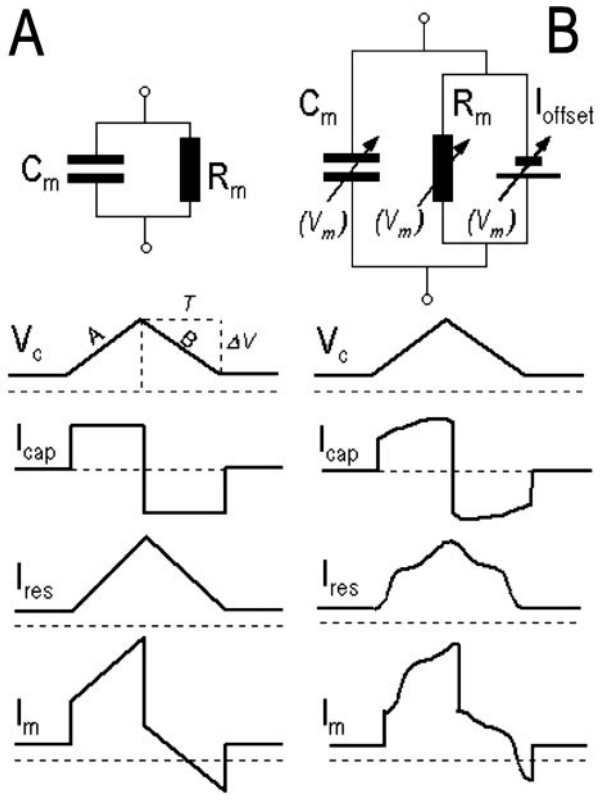

FIGURE 2 Principle of capacitance measurements using paired voltage ramps. (*Upper*) Electrical equivalent circuit of hypothetical cells; (*Lower*) Voltage stimulus and corresponding current components. (*A*) Passive, linear network. Membrane capacitance C_m and resistance R_m can be determined theoretically exact from the current integrals during the ramps A and B, together with the known ramp duration T and ramp height ΔV. (see Methods for details); (*B*) Active, nonlinear network. In addition to *A*, an energy source producing an offset current I_{offset} is present, and the respective values of all elements are functions of membrane potential V_m. If C_m is not constant within the tested voltage range, the calculated C_m represents the corresponding average (see Methods for details). V_c, command voltage; I_{cap}, capacitive current component; I_{res}, current across R_m (in *A*) or across R_m plus I_{offset} (in *B*); I_m, total membrane current.

magnitudes of C_m, R_m, and I_{offset} are not assumed to be constant but may vary as functions of V_m. Interestingly, C_m can still be determined by the same procedure, even though the particular voltage dependencies of all three elements may be unknown (assuming time independence of all variables; see Discussion). This follows intuitively from the consideration that voltage dependence changes only the shape of the capacitive and resistive current components, but not their symmetry around a point and a mirror axis, respectively. Therefore, Eqs. 1–3 are satisfied again, which define C_m unambiguously (Eq. 4). If C_m itself varies between V_{hold} and V_{peak} as a function of V_m, the calculated value of C_m acquires the meaning of the average capacitance between these two points.

Ramp stimulus

The calculation of C_m is independent from the nature of the stimulus segments preceding and following the relevant ramp segments. It is therefore possible to embed the relevant ramp segments of the voltage stimulus in other segments. These can be designed such that they 1) do not cause sudden current jumps by themselves, 2) last long enough to sufficiently diminish the effect of preceding jumps, and 3) challenge only minimally the voltage clamp with respect to speed and current amplitude. These measures will help to minimize the effect of clamp artifacts, non-ideal clamp behavior, or slow clamp (Fig. 3 *A*).

Further important ramp parameters are the slope dV/dt, duration T, and position, defined by V_{hold}. Under ideal voltage clamp conditions, the capacitive component of the compound current increases linearly with dV/dt, improving the signal-to-noise ratio, whereas the total signals (i.e., Q_A and Q_B) increase with t, improving precision. In this work, ramps had slopes of 2 V/s and durations of 10 ms as shown in Fig. 3 *A*, and V_{hold} was set to −50 mV, unless indicated otherwise.

Monitoring of other electrical parameters

In many experiments, it is desirable or required to not only collect C_m information but also cover the other electrical parameters of biomembranes as well. For instance, to fully describe a lumped parameter equivalent circuit of a rather simple model cell, consisting of a capacitance, a parallel conductance, and a parallel current source (or, equivalently, a voltage source in series), two further variables need to be determined in addition to C_m. In principle, this could be done by sampling I_{hold} at V_{hold} as point measurements during a constant voltage segment between two ramp stimuli and calculating G_m from the paired ramps as $G_m = (Q_A + Q_B)/T(2V_{hold} + \Delta V)$. In practice, however, we observed in preliminary experiments that this approach yielded noisy and inaccurate results, particularly when G_m was small and C_m large.

Better results were obtained by using a second, separate voltage stimulus and apply again signal averaging to the resulting current trace. This stimulus (Fig. 3 *A*, *lower panel*) consists of a simple step from $V_{hold}(1)$ to $V_{hold}(2)$. Averaging of I_m over the same time windows as for the paired ramps yields $I_{hold}(1)$ and $I_{hold}(2)$. These *I-V* pairs define two points that are sufficient to completely determine a linear *I-V* relationship, implying the values of R_m, G_m, slope conductance g_m, r_m (the reciprocal of g_m), and the reversal potential E_{rev}. Furthermore, C_m together with a value for specific capacitance from the literature (e.g., ~1 μF/cm^2) may be used to calculate membrane surface area A and hence the scalar current density $J = I_m/A$.

Software

Two commercially available electrophysiology software programs, PULSE and X-CHART (HEKA Electronics, Lambrecht, Germany), were programmed to carry out stimulation, data acquisition, signal averaging, C_m calculation, and display of raw traces and calculated C_m values (Fig. 3). The important feature herein is the integration of two complementary programs: one of them (PULSE) samples raw current data at high rates (50 kHz) but subsequently reduces this complex information to a few characteristic parameters, i.e., Q_A and Q_B, or $I_{hold}(1)$ and $I_{hold}(2)$, using the online analysis function. The second program (X-CHART) samples the results of the first program's online analysis at low rates (<50 Hz) and virtually in real time and uses them together with the known stimulus parameters to calculate C_m, g_m, E_{rev}, etc. Thus, the high-frequency data can be discarded after every sweep. This integrated mode of operation minimizes data load and offers great flexibility with respect to real-time calculations and display.

Hardware

For two-electrode voltage-clamp experiments, we used a TEC-05 amplifier (NPI Electronic, Tamm, Germany) that was connected to a personal computer via an analog-digital converter (ITC-16; Instrutech, Port Washington, NY). Clamp performance was adjusted according to the absolute value optimum (AVO) algorithm (Polder and Swandulla, 2001) by means of proportional and integral gain controls during application of a square-

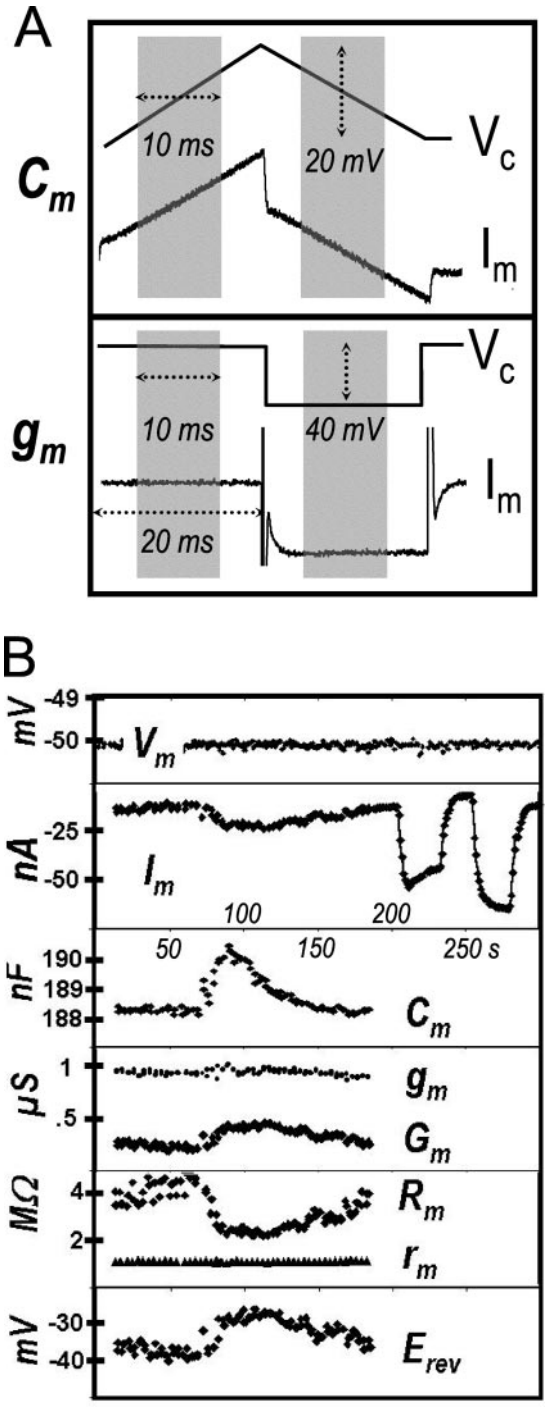

FIGURE 3 Paired ramps plus step protocol allow comprehensive monitoring of electrical parameters. (*A*) Voltage stimuli and current responses. (*Upper panel*) C_m: determination of capacitance; (*Lower panel*) g_m: determination of current-voltage relationship. V_c, voltage stimulus; I_m, current response (original recordings from an untreated stage V *Xenopus* oocyte), shaded areas, windows for integration (C_m) or averaging (g_m). C_m is calculated from the two current integrals as described in Methods. g_m is calculated as the difference of the two average currents, divided by the height of the voltage step. (*B*) Comprehensive equivalent circuit monitoring. Sample recording, illustrating the continuous monitoring of equivalent circuit parameters (C_m, V_m, I_m, G_m, g_m, R_m, r_m, E_{rev}; see Methods) from the two alternatively applied stimuli, taken from ongoing studies on the role of cysteines in the electrogenic, polyspecific organic cation transporter from rat (rOCT1). At ~60 s, the oocyte was exposed for 50 s to 5 mM MMTS, a membrane-permeable, covalent cysteine modifying reagent. At 180 s, current filtering was switched from 20 kHz to 20 Hz, and I_m was sampled directly from the current output of the amplifier. At 200 and 250 s, the oocyte was superfused with substrates of rOCT1 (3 mM TEA and 10 mM choline, respectively). Noise in the I_m trace is of similar magnitude with averaging at 20 kHz as compared with individual data points from the heavily filtered (20 Hz) I_m trace. A transient C_m increase of ~2 nF is clearly resolved. Furthermore, it can be seen that in this example I_m is not following g_m, but rather changes due to a changing E_{rev}. Some parameters are not independent variables, but helpful for visualization, e.g., g_m versus r_m.

shaped control pulse. Herein, the integral portion of the feedback circuit reduces the steady-state voltage clamp error to zero, both in theory and in practice (Polder and Swandulla, 2001). Neither capacitance compensation nor series resistance compensation were used throughout this study. Current signals were filtered at 20 kHz using a four-pole Bessel filter.

For voltage clamping of the model cell, the current and potential electrode holders and ground were directly connected with the model via BNC adapters or plugs, respectively. For voltage clamping of *Xenopus* oocytes, cells were placed in a small, custom-made Teflon chamber and impaled with microelectrodes that were filled with 3 M KCl and had final resistances of 0.5–2.0 MΩ (current electrode) or 1–5 MΩ (potential electrode). Silver wires for microelectrodes and ground wires were chlorided in 3 M KCl under standardized conditions using a chloriding apparatus (NPI Electronic). The TEC-05 functions as a voltage-controlled current source (Polder and Swandulla, 2001; Kordas et al., 1989), and the bath could be grounded directly by a AgCl wire without a bath clamp. The *Xenopus* oocytes could be superfused continuously through a gravity-fed system. For quick solution changes, solutions were pipetted directly into the chamber.

Electrical cell model

To assess the performance of our method to measure capacitance in *Xenopus* oocytes, we relied largely, but not exclusively, on a model electrical circuit (Fig. 4). Most measures of analytical performance, e.g., accuracy, precision, and robustness in the face of varying recording conditions, cannot be characterized directly in *Xenopus* oocytes in a reproducible and comprehensive way. First, the true value of C_m (and of other relevant electrical parameters) in *Xenopus* oocytes is unknown, and no gold standard is currently available that could be used to calibrate these preparations. Second, the electrical parameters of the membrane and the recording arrangement cannot be manipulated individually and randomly to test a range of defined recording conditions. These limitations can be overcome with an appropriate model circuit.

We used a model circuit in which the oocyte is represented as a three-element network (Fig. 4), consisting of a series resistance (R_s) that is connected in series with a parallel combination of a membrane resistance (R_m) and a membrane capacitance (C_m). The model circuit furthermore includes fixed current electrode and potential electrode resistances (1 MΩ each), and fixed bath and reference electrode resistances (100 kΩ each). The model was assembled from a custom-built circuit (NPI Electronic, Tamm, Germany) with infinitely tunable R_s and R_m (0–2 kΩ and 0–2 mΩ, respectively) and a capacitance box that allowed us to set C_m values between 0 and 1000 nF in 10-pF steps (Martindale Electric, Watford, UK).

Xenopus oocyte experiments

For performance tests in *X. laevis* oocytes, we used native stage V-VI oocytes. Animal husbandry, partial ovariectomy, defolliculation, cRNA

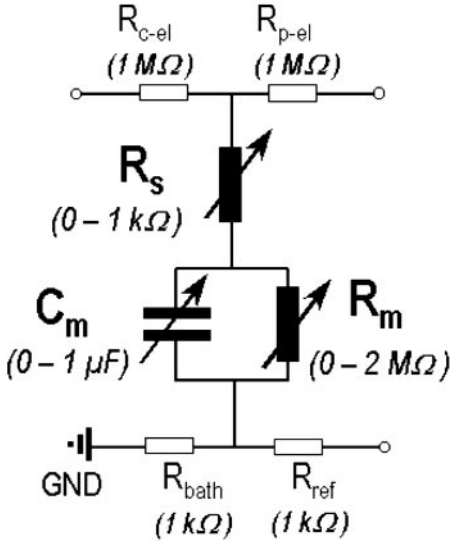

FIGURE 4 Electrical cell model used to test C_m determination using paired voltage ramps. An electrical circuit with individually tunable parameters, representative of a typical arrangement for two-electrode voltage-clamp (TEVC) recording from *Xenopus* oocytes, was used to quantitate accuracy, precision, and robustness of C_m measurements (see Methods for details). R_s, series resistance; R_m, membrane resistance; C_m, membrane capacitance; $R_{c\text{-}el}$, current electrode resistance; $R_{p\text{-}el}$, potential electrode resistances; R_{bath}, bath electrode resistance; R_{ref}, reference electrode resistance.

synthesis and injection, and maintenance of oocytes was performed by standard procedures as described previously (Nagel et al., 1997). ND96 solution consisted of 94 mM NaCl, 2 mM KCl, 1 mM $MgCl_2$, 1.8 mM $CaCl_2$, and a combination of 1.953 mM HEPES acid and 3.047 mM sodium HEPES, yielding pH 7.4 at 22°C. Phorbol-12-myristate-13-acetate (PMA) and 8-Br-cAMP were purchased from Sigma Chemicals (Deissenhofen, Germany) and methyl-methane-thiosulfonate (MMTS) from Toronto Research Chemicals (Toronto, Canada).

RESULTS

Continuous monitoring of C_m using our modified ramp approach was implemented in PULSE and X-CHART with a few short files (available from the authors). These files defined the stimulation protocols (pulse generator file, *.pgf), the online analyses (macro file, *.mac), and C_m calculation and data display (parameter file, *.prm). C_m monitoring was started and stopped via a button in the oscilloscope window of PULSE. Random activation and deactivation of C_m measurements during an experiment was possible without data loss, which allowed, for instance, to run other protocols such as *I-V* curves or to switch intermittently to current clamp mode. During C_m measurements, the I_m responses to the voltage stimuli were displayed in the oscilloscope window, providing visual feedback about clamp quality. In two further windows, X-CHART displayed basic parameters and online-analysis results sampled from PULSE (V_c, V_{hold}, I_m, I_{hold}, and Q_A, Q_B, $I_{hold}(1)$, $I_{hold}(2)$, respectively) and derived parameters calculated by X-CHART (C_m, R_m, r_m, G_m, g_m, E_{rev}, *A*, and *J*), both as continuous traces (graph window) and in numerical form (data and comments window; Fig. 3). These values were continuously updated in real time, and no off-line analysis was required.

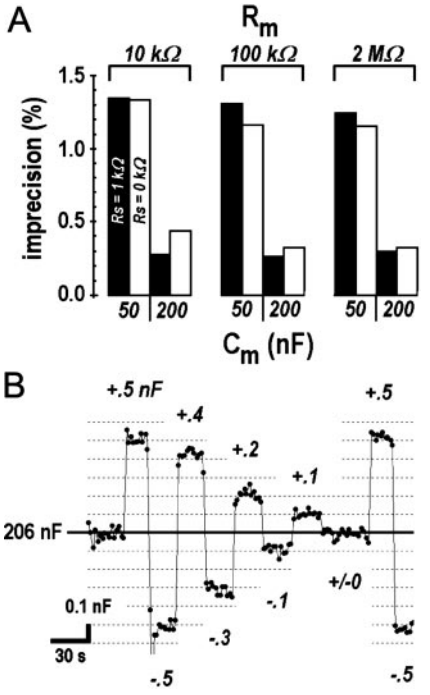

FIGURE 5 Precision of C_m measurements using paired voltage ramps in electrical cell model. (*A*) Imprecision of individual C_m estimates at 50 nF and 200 nF. Imprecision is given as the coefficient of variation (in percent) of C_m measurements as estimated from 100 paired ramp duplets for each data point (*bars*). Measurements were obtained for both C_m values at various R_m (10 kΩ/100 kΩ/2 MΩ) and two different R_s (0 Ω/1 kΩ). It can be seen that imprecision increases at smaller values of C_m, whereas R_m and R_s do not affect precision within the tested range. (*B*) Resolving 0.1-nF differences using signal averaging. C_m of the model circuit was set to ~206 nF, and small deviations from this value were superimposed by means of a dial with a 100-pF gradation. Each data point was averaged from 20 individual C_m determinations. Averaging required for this sensitivity reduces time resolution to ~0.5 Hz.

Precision in model circuit

Fig. 5 shows the results of measurements in the model cell that should test the precision of the method. The quantitative measure used here to describe the variability of individual C_m determinations was the coefficient of variation (in percent), or relative imprecision.

It can be seen in Fig. 5 *A* that imprecision of C_m estimates was smaller than 1.4% under all tested conditions. Relative imprecision was smaller at higher C_m as compared with lower C_m (0.27–0.44% at 200 nF vs. 1.16–1.35% at 50 nF). In absolute values, however, imprecision was comparable in both cases (500–800 pF). Interestingly, imprecision was not significantly affected by R_s or R_m (Fig. 5 *A*).

As expected, precision could be improved by averaging C_m from multiple measurements. Fig. 5 *B* shows a recording where each data point was averaged from 20 individual C_m estimates; starting with a capacitance of ~206 nF, C_m was changed in steps of decreasing magnitude (R_s = 0 kΩ, R_m = 2 MΩ). It can be seen that this moderate averaging was sufficient to reliably resolve changes of 100 pF, corresponding to a resolution of ~0.05%. At this improved sensitivity, C_m updates were obtained approximately every 2 s or at 0.5 Hz, as opposed to ~0.05 s or 20 Hz without averaging.

With the second, voltage-step protocol, the absolute imprecision of individual I_{hold} measurements was rather constant around ±5 nA, which translated into relative imprecision that depended strongly on R_m (0.09% at 10 kΩ, 0.10% at 100 kΩ, and 9.78% at 1 MΩ; n = 1000, R_s = 0 Ω, and C_m = 250 nF).

Accuracy in model circuit

Fig. 6 shows the results of measurements that should test the accuracy of the method in the model cell. The quantitative measure used was inaccuracy, i.e., the deviation of measured C_m from the true C_m, expressed in percent of the true C_m.

In the absence of any series resistance (Fig. 6, *top panel*), inaccuracy of the C_m estimates was ≪1% for most conditions tested. Values above that band were found when C_m was very small (<50 nF). Inverting the orientation of the test pulse did not affect C_m determination. Initial experiments had shown an increasing underestimation of C_m with decreasing C_m (data not shown). This effect could be attributed to a phase lag, introduced by the four-pole Bessel filter, which in effect shifted the current integration window off the ramp center. The error was largely abolished after shifting the integration window into the same direction by 40 μs, the measured value of the phase lag. Alternatively, direct sampling of the unfiltered current output abolished these systematic deviations, but this approach was associated with increased imprecision, probably due to aliasing noise.

We noted that such high accuracy of C_m measurements depended on the use of proportional-integral feedback, afforded by the TEC-05 amplifier, as compared with simple proportional feedback. For instance, when integral gain was switched off and proportional gain set to maximum, we observed underestimation of a 250-nF capacitance by ~5% at R_m = 10 μΩ and of ~0.25% at R_m = 100 kΩ. With proportional gain deliberately reduced to yield a steady-state clamp error of 5% at V_c = −100 mV and R_m = 10 kΩ, the resulting C_m errors were greater than expected from the clamp error alone (~10% at 500 nF, ~8% at 250 nF, ~7.5% at 150 nF, and ~9% at 50 nF). With integral gain switched on, the C_m estimates became virtually identical to the ones obtained with maximized proportional gain (Fig. 6).

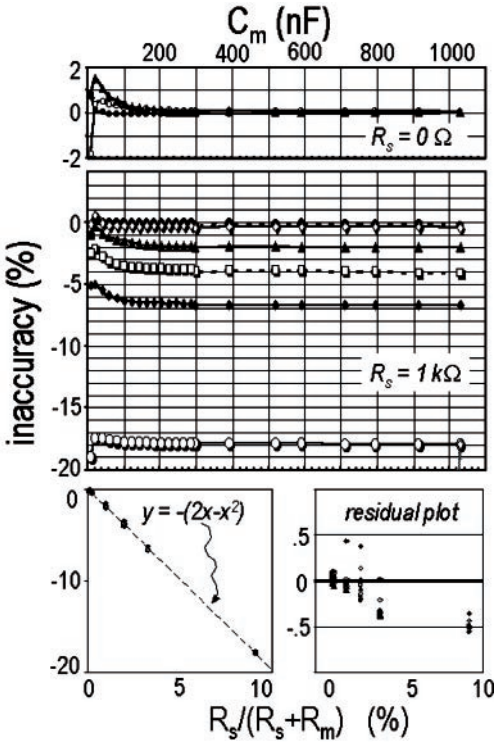

FIGURE 6 Accuracy of C_m measurements using paired voltage ramps in electrical cell model. Inaccuracy of C_m measurements was measured as the difference (expressed in percent, *ordinate*) between the C_m value dialed on the model circuit (*abscissa*) and the measured C_m value (mean, n = 200 for each data point). (*Upper panel*) Series resistance R_s = 0 Ω; (*middle panel*) R_s = 1 kΩ; various values of membrane resistance R_m (10 kΩ, ○; 30 kΩ, ♦; 50 kΩ, □; 100 kΩ, ▲; 500 kΩ, ◇; 1 MΩ, ●) and of C_m (10–1000 nF, *abscissa*). For R_m ≥ 100 kΩ, inaccuracy of C_m estimates was better than −2% under all conditions, irrespective of R_s. (*Left bottom panel*) Plot of inaccuracy (in percent) as a function of $R_s/(R_s + R_m)$, expressed in percent; dashed line is the plot of the fitted function $y = -(2x - x^2)$; (*Right bottom panel*) residual plot showing the deviation of observed inaccuracy from the fit. Similarly small residuals are obtained with $y = -2x$.

With series resistances of 0.5 kΩ (not shown) or 1.0 kΩ (Fig. 6, *middle panel*), systematic underestimation of C_m became apparent also with proportional-integral feedback. This underestimation reached from a few percent to more than 17% at R_m = 10 kΩ. If R_m was 100 kΩ or higher, however, inaccuracy was always better than −2%. The empirically obtained errors very closely followed the theoretically predicted errors (Fig. 6, *lower panels*; see *Discussion*).

With the second, step protocol, the inaccuracy of individual g_m estimates was smaller than the 1% tolerance of the resistors used to build the model cell (0.5, 1.0, 10, and 100 μS). Because g_m is calculated from the difference between two I_{hold} values, it was independent from putative offset currents. In contrast, the accuracy of individual I_{hold} measurements was limited in practice by the relatively coarse dial used to zero the I_m output of the amplifier.

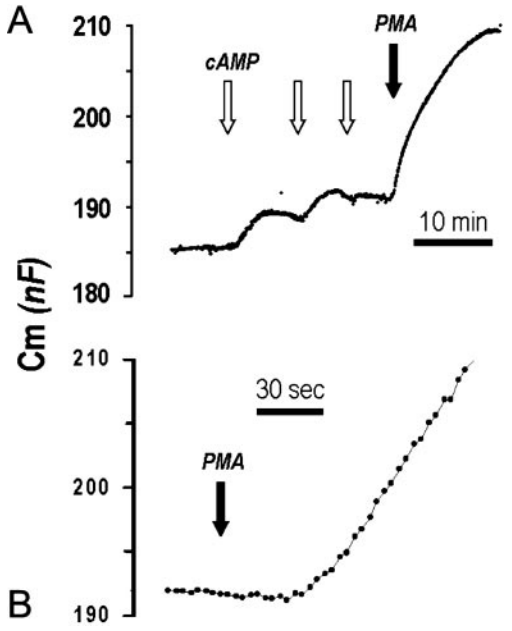

FIGURE 7 Measuring small and fast C_m changes in *Xenopus* oocytes using paired voltage ramps. (*A*) Effect of cAMP on C_m in native *Xenopus* oocyte. White arrows indicate 100-s incubations in 100 μM 8-Br-cAMP, and black arrow indicates 100-s incubation in 1.0 μM phorbol-12-myristate 13-acetate (PMA). The findings suggest that PKA and PKC regulate two distinct pools of potential exocytotic vesicles. (*B*) Effect of PMA on C_m in native *Xenopus* oocyte. Arrow indicates 100-s incubation in 1.0 μM PMA. Assuming diameters of the exocytotic vesicles of 180 nm, corresponding to 0.8 fF, the observed exocytosis rate implies ~375,000 fusion events per second. Here, voltage ramps with a downward slope of 1 V/s were used (cf. Fig. 3 *A*).

Performance in *Xenopus* oocytes

In *Xenopus* oocytes, C_m was recorded with the same protocol as used with the model circuit. Continuous stimulation for up to 2 h did not affect stability or quality of the recordings, as judged from baseline electrical parameters and C_m values. Imprecision in *Xenopus* oocytes was comparable to imprecision in the model cell; no attempt was made, however, to evaluate imprecision in relation to C_m, R_m, or R_s in a systematic manner. Accuracy could not be tested in *Xenopus* oocytes. In contrast to the model cell, inverting the orientation of the test pulse slightly and inconsistently reduced the apparent C_m. This effect was only observed when pulses started from the same V_{hold} into opposite directions but was abolished when V_{hold} was adjusted such that the voltage range covered during the integration windows was identical for upward and downward pulses. These observations point to a genuine voltage dependence of C_m rather than an artifact, but this was not pursued further.

Fig. 7 *A* shows that our method resolved C_m changes in the nF range. An oocyte continuously superfused with ND96 control solution showed a stable baseline capacitance of ~185 nF. Upon exposure to 100 μM 8-Br-cAMP in ND96 for 100 s, membrane capacitance initially increased within several minutes by ~5 nF to a new stable value. Upon repeated exposure, a smaller increase of ~3 nF was observed, and a third pulse of the cAMP analog failed to produce a significant effect on C_m. In contrast, subsequent incubation in 1 μM PMA produced a large C_m increase of ~20 nF within ~10 min, followed by a prolonged C_m decrease (not shown). Similar effects of cAMP, both qualitatively and quantitatively, were observed consistently in other oocytes tested. These findings suggest that PKA activation can mobilize only a small subset of potential exocytotic vesicles, whereas PKC activation controls a larger vesicle pool. It is unclear whether cAMP-dependent and PMA-dependent vesicle pools are completely distinct or whether they partially overlap. Such data on repeated or successive stimulations in a single cell would be hard to obtain using biochemical approaches.

Fig. 7 *B* illustrates that our method was able to monitor relatively fast C_m changes. The C_m change was produced by incubation of the oocyte in 1 μM PMA and became apparent after a lag phase of ~30 s. The C_m increase was followed by a prolonged and sustained C_m decrease (not shown). Time resolution and precision allow us to determine the rate of C_m change (dC_m/dt); in this experiment, the maximal rate was ~0.3 nF/s, corresponding to net addition of plasma membrane surface area of 0.03 μm^2/s. Assuming a diameter between 60 and 180 nm per single exocytotic vesicle (corresponding to a capacitance between 0.1 and 0.8 fF), the number of fusion events per second should be between 375,000 and 3,000,000. Qualitatively similar results were obtained in experiments on several other oocytes. The duration of the lag phase in this experiment (Fig. 7 *B*) was representative, but the net rate of exocytosis was higher than average. Again, it would be difficult to measure such rates of endo-/exocytosis in single cells using biochemical assays.

Fig. 8 shows that our modified ramp approach also allows us to follow complex and long-lasting C_m changes. Here, a representative C_m trace illustrates the rather stereotypical response of *Xenopus* oocytes to 100-s incubation in 1 μM PMA: starting from a stable baseline C_m value of ~200 nF, C_m increased rapidly by ~10 nF but then fell continuously for at least 60 min to C_m values less than half of the baseline value. Notably, apart from the 100-s incubation (*arrow*), PMA was absent throughout the experiment.

The pattern of a limited initial C_m increase followed by a long and pronounced C_m decrease was consistently observed in control oocytes ($n = 30$) from several donor animals. For the C_m decrease, the maximum rates were rather constant ($\sim -6 \pm 2$ nF/min). Therefore, measurements of net endocytosis rate in response to a PMA pulse can be used as a marker for the functional state of an oocyte's endocytosis machinery. Using this strategy, we could identify a pronounced effect of the regulatory protein

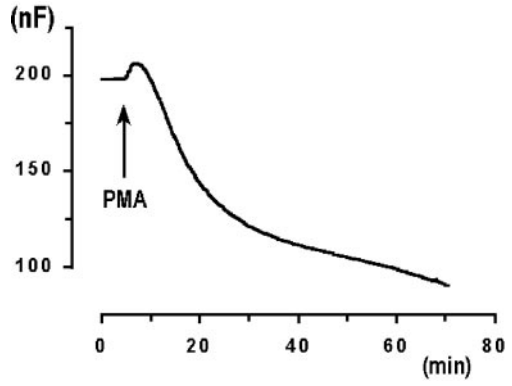

FIGURE 8 Measuring complex and long-lasting C_m changes in *Xenopus* oocytes using paired voltage ramps. Effect of PMA on C_m in native *Xenopus* oocyte. Arrow indicates 100-s incubation in 1.0 μM PMA, which was preceded and followed by continuous superfusion with ND96. Ramps were as in Fig. 7. Without PMA treatment, C_m of *Xenopus* oocytes does not change significantly within similar time periods (data not shown). In contrast to patch clamp or other approaches, such slow and prolonged changes of membrane surface area can be followed conveniently by C_m measurements in *Xenopus* oocytes. The pronounced effect of PMA illustrates the importance of C_m monitoring when studying the hormonal regulation of ion channels or transporters. Because the effects are complex and time dependent, end-point measurements may be misleading, as opposed to continuous monitoring.

RS1 on PMA-stimulated endocytosis rate (M. Veyhl, B. M. Schmitt, and H. Koepsell, unpublished results).

DISCUSSION

This work introduces paired voltage ramps as a method for the continuous monitoring of membrane capacitance (C_m). The method allows accurate, precise, robust, and simple monitoring of C_m in large cells such as *X. laevis* oocytes using the two-electrode voltage-clamp technique. In combination with a second pulse protocol, the complete electrical parameters of an equivalent circuit comprising parallel capacitance, conductance, and current source (or, equivalently, a serial voltage source) can be monitored. Though not tested explicitly, this approach could also be adopted in patch clamping. This should be particularly straightforward, for instance, for the whole-cell mode for which efficient techniques to handle R_s issues already exist (Sherman et al., 1999).

Precision

High precision of C_m measurements is required to obtain low-noise recordings and to resolve small C_m changes reliably. In practice, hormones or second messengers may produce C_m changes of only few nF in *Xenopus* oocytes (Vasilets et al., 1990; Loo et al., 1996; Wright et al., 1997), making a resolution of ~1 nF or better desirable. The method will be taxed even more by studies of gating currents, ion binding steps, conformational changes of membrane transporters, or effects of exogenous hydrophobic ions.

The precision of our modified ramp approach affords 1-nF resolution even under rather difficult recording conditions (Fig. 5 *A*). Averaging of several individual C_m measurements further improves precision (Fig. 5 *B*).

The precision of approaches using step commands in *Xenopus* oocytes has not been reported. In contrast, the precision of admittance-based C_m measurements using patch-clamp techniques has been studied in great detail and optimized close to the theoretical limits (Gillis, 1995, 2000; Lollike and Lindau, 1999; Chen and Gillis, 2000). In absolute terms, inaccuracy increases with membrane area, with values being lowest in excised patches and significantly higher in the whole-cell configuration. In relative terms, imprecision in a 22-pF model circuit under optimum conditions was ~0.05%, corresponding to ~10 fF (Gillis, 1995). Thus, relative imprecision of patch-clamp-based admittance measurements is virtually identical with the imprecision of our paired ramp approach (Fig. 5 *B*), and both methods probably are similarly close to their theoretically achievable limits.

Accuracy

Accuracy (or fidelity) pertains to the absolute value of the measured C_m and its deviation from the true C_m value. Thus, accuracy is clearly the most important aspect of performance when the absolute value of C_m is the parameter of interest, e.g., estimation of membrane permittivity or total surface area. In fact, however, accuracy is of equal importance when only relative changes are studied (see under Robustness below).

In the absence of series resistance, our modified ramp approach yields very accurate C_m estimates over the entire range (and beyond) of C_m and R_m values encountered in TEVC experiments on *Xenopus* oocytes: 10 kΩ < R_m < 2 MΩ, 10 nF < C_m < 1000 nF (Fig. 6). When a series resistance is present, it is expected that the apparent C_m value, C_m^*, will deviate from the true C_m in a systematic way. The relative error $\varepsilon = (C_m^* - C_m)/C_m$ can be calculated from the time course of $V_m(t)$ in the model circuit (Fig. 4), given as $V_m(t) = (dV/dt) \times [R_m/(R_s + R_m)] \times [t - R_i \times C_m(1 - e^{-(R_i \times C_m)}]$; herein, R_i represents $R_s \times R_m/(R_s + R_m)$, the parallel combination of R_s and R_m. Neglecting the exponential term, ε is approximated by $\varepsilon \approx 2 \times R_s/(R_s + R_m) - [R_s/(R_s + R_m)]^2$, or simply and still sufficiently accurate as $\varepsilon \approx 2 \times R_s/(R_s + R_m)$. Our finding of an excellent agreement between predicted and observed errors (Fig. 6, *bottom panels*) has two important implications. First, the effect of uncompensated series resistance can probably be neglected in most experiments. To measure C_m with less than 2% inaccuracy in *Xenopus* oocytes, where R_s is usually less than 1 kΩ, conductances as high as 10 μS can

be tolerated (Fig. 6). This limit allows us to study safely electrogenic transporters or pumps but may preclude C_m measurements in oocytes with overexpressed, fully activated ion channels. Second, the tight correlation of the error with the ratio $R_s/(R_s + R_m)$ suggests that this source of inaccuracy can be largely eliminated if R_s is known from an independent measurement, allowing us to monitor C_m even under such extreme conditions. Methods for fast and accurate measurement of R_s in *Xenopus* oocytes are unavailable at present but under way (H.-R. Polder, personal communication).

A unique advantage of the paired ramps is that they yield accurate C_m estimates irrespective of whether the *I-V* relationship is linear or nonlinear, provided the *I-V* relationship is not time varying (Fig. 2). Charges moved due to such nonlinear current components are perfectly canceled out by the algorithm used to calculate C_m. Therefore, voltage-dependent activation or inactivation of conductances per se do not affect the C_m measurements. For instance, our approach would probably yield valid C_m estimates in *Xenopus* oocytes expressing channels with rapid and simple voltage gating such as certain twin-pore K^+ channels (Rajan et al., 2001). Similarly, the contribution of gating charges per se to the true C_m of a given real membrane under investigation would yield a correct value of what could be termed the chord capacitance of a nonlinear capacitor over the particular voltage interval tested.

In contrast, when activation and inactivation of conductances occur over finite periods, possibly in complex patterns, C_m estimates will not be exact any more. The magnitude of the error depends on the pattern and time constants of the gating processes, the magnitude of the activated or inactivated conductances, and the amplitude and position of the ramp stimulus. In general, it is therefore usually best to place the stimulus outside the range where membrane conductance is voltage sensitive. If this is not possible or desired, however, the paired ramp approach will, in contrast to the other methods, at least tend to minimize the effect of such nonlinearities and thus enhance the robustness of the C_m measurements.

The accuracy of C_m determinations using step commands has not been assessed systematically. The basic version (Lindau and Neher, 1988; Vasilets et al., 1990; Hirsch et al., 1996; Forster et al., 1999; Gentet et al., 2000) will return inaccurate C_m estimates if the approximation $Q_{res} = I_m(t\rightarrow\infty) \times t$ is not valid. Approaches that incorporate the assumption that both I_{res} and I_{cap} follow monoexponential time courses with the same time constant τ_1 and use numerical or other methods or to solve for Q_{res} and Q_{cap} will be more exact (Adrian and Almers, 1974; Peres and Bernardini, 1985) (pCLAMP 8.0 software, Axon Instruments, Foster City, CA). However, step protocols are intrinsically sensitive to filtering, nonlinear series resistance or current electrode resistance, oscillations, and slow clamp, and the presence of systematic errors is not always easy to detect.

An additional, more fundamental concern with C_m determinations based on time constants is the underlying assumption that the current decay is perfectly monoexponential. This assumption can be tested directly using electronic transient neutralization (Gillis, 1995). It was found in *Xenopus* oocytes that fitting the transient with up to three different time constants suppressed no more than 90–95% of the transient amplitude (Stühmer, 1998; H.-R. Polder, personal communication). Taken together, it is unlikely that accuracy and robustness of step approaches are equal to or better than that of ramp protocols.

The accuracy of admittance-based methods has not been addressed explicitly, either for the more popular patch-clamp approaches or for the TEVC variety (Weber et al., 1999; Awayda, 2000). For the patch-clamp version, inaccuracy is estimated to be ~5–10% in expert hands (K. D. Gillis, personal communication), and may be similar for the TEVC variety.

Time resolution

In most studies of C_m in *Xenopus* oocytes, C_m was measured discontinuously at one or several time points (Moody and Lansman, 1983; Moody and Bosma, 1985; Peres and Bernardini, 1985; Block and Moody, 1987; McCulloh and Levitan, 1987; Vasilets et al., 1990; Hirsch et al., 1996; Zhu et al., 1997; Forster et al., 1999), rather than monitoring C_m continuously throughout the course of the experiment (Weber et al., 1999; Awayda, 2000). Discontinuous C_m measurements provide less information, however, and may give rise to false conclusions.

The maximum frequency with which the paired-ramp approach can generate C_m estimates is determined by the duration of the ramp stimulus (Fig. 2). In practice, stimuli should probably not be shorter than 20 ms, corresponding to a maximum frequency of 50 Hz. Averaging C_m over several stimulation cycles will proportionally decrease the time resolution. For instance, if 100-pF changes need to be resolved, time resolution drops to ~0.5 Hz (Fig. 5 *B*).

With step commands, time resolutions ranging from 2 s to minutes were reported (Peres and Bernardini, 1985; Quick et al., 1997; Peters et al., 1999; Tong et al., 2001). Higher rates with step commands have been achieved in *Aplysia* neurons (~60 Hz (Johnson and Thompson, 1989)) and with continuous triangular voltage ramps in squid giant axon (~900 Hz (Palti, 1969)). The theoretically achievable time resolution with step commands is similarly limited by the time required to cover the response to the step command completely. In practice, six to eight time constants will be the minimum. In TEVC experiments on *Xenopus* oocytes, the upper limit under optimal clamp conditions is probably ~50 Hz.

Admittance-based methods can provide outstanding time resolution of up to several kilohertz in small cells (Lindau and Neher, 1988). In *Xenopus* oocytes, however, the theo-

retical and practical limits are significantly lower (Weber et al., 1999; Awayda, 2000).

On the other hand, there would probably be no tangible benefit in increasing the time resolution of C_m measurements beyond several hertz. The only known example for fast C_m changes is the fusion of single exocytotic vesicles. Unfortunately, even with sufficient time resolution those fusion events cannot be resolved in whole *Xenopus* oocytes because the associated C_m changes are by many orders of magnitude smaller than thermal noise (Gillis, 1995).

Robustness

Practically relevant aspects of robustness are accuracy in the face of variable R_s and R_m, precision in the face of variable R_s and R_m, and accuracy in the face of non-ideal clamp conditions. In the absence of series resistance, the accuracy of our method is extremely robust in the face of R_m changes (Fig. 6). If clamp fidelity or speed is insufficient, however, R_m decreasing to very low values may cause an apparent C_m decrease (see Results). This is probably more a question of designing feedback controllers, rather than a problem of our method, because such artifacts are virtually absent when proportional-integral feedback is used (Fig. 6), as compared with proportional feedback only (see Results). If C_m is determined without integral feedback, it is important to use the highest proportional gain that is compatible with clamp stability and to observe the steady-state voltage error as a rough estimate of the concurrent C_m error.

In contrast, the changes of R_m in the presence of a series resistance compromise accuracy in an unavoidable and predictable fashion. Therefore, fluctuations of R_s or R_m can mimic C_m changes. Such R_s errors are often difficult or impossible to detect or to quantitate. Fortunately, it follows from the exact quantitative relationship (see above, Discussion) that rather large fluctuations are required to produce significant errors. Furthermore, methods for fast and accurate monitoring of R_s may allow elimination of such errors in future. On the other hand, when the working range will be extended with the aid of such methods to include very high currents (>20 μA), it will become necessary to verify explicitly the assumption of perfect space clamp (isopotentiality) and take appropriate measures to minimize isopotentiality errors, if necessary (Baumgartner et al., 1999).

Precision, on the other hand, was found to be largely unaffected by changes of R_s or R_m. Finally, robustness in the face of non-ideal clamp conditions is difficult to assess quantitatively. We observed, however, that C_m readings remained remarkably stable when the clamp was very slow or even when oscillations occurred, conditions under which neither voltage step nor sine wave commands would yield useful results.

Ease of implementation and operation

Implementation of our modified-ramp approach requires standard TEVC instrumentation interfaced with a personal computer, two commercially available electrophysiology programs (PULSE and X-CHART), and a few short files that define pulse shape, online analysis, C_m calculation, and display modes. Acquisition of C_m together with the other electrical parameters does not require any modifications of the standard TEVC recording arrangement and can be activated by a simple command. As long as the recording arrangement is stable, operation can proceed automatically. In particular, neither the experimenter nor the software needs to keep track of any parameters.

During C_m measurements using our modified-ramp approach, the individual current responses to the ramp stimulus are displayed in a separate window of PULSE (oscilloscope). Characteristic features of the current trace provide a direct visual representation of C_m and R_m. Potential problems with clamp quality, such as slow clamp, oscillations, etc., are thus apparent and can be corrected immediately during the experiment.

With step commands, hard- and software requirements are probably comparable, albeit computing overhead is higher with the time constant approach because of the curve fitting procedures. Automatization should be possible in a similar way but has not been implemented for TEVC experiments to date.

Admittance-based C_m measurements in the TEVC mode, in contrast, may require extra hardware, such as a second A/D converter or a sine-wave generator (Weber et al., 1999). Moreover, no standard software is available for data handling and processing, including the complex transforms and fitting procedures. Importantly, the validity of C_m measurements based on admittance methods depends on a rather high number of parameters, including gain, amplitude, frequency, and digitization of the sine wave stimulus, filtering of stimulus and current signal, and the settings for capacitance and series resistance compensation (Gillis, 1995). Their individual and combined effects on the C_m determinations are complex, and errors due to incorrect settings are not immediately obvious. Clearly, a high level of theoretical knowledge and familiarity with admittance measurements in particular are necessary to obtain valid C_m data with these methods.

Taken together, our modified-ramp approach is suited to monitor C_m in *Xenopus* oocytes with high accuracy, precision, and robustness. Moreover, our method is well characterized, simple, inexpensive, and easy to use. Based on available data, the performance of our approach is equal or superior to other TEVC approaches. Analysis of the other approaches furthermore shows that their theoretically achievable performance is not significantly different from the performance already available with our method. C_m measurements can be conveniently combined with a step

pulse to allow simultaneous monitoring of V_m and I_m as well as of important additional electrical circuit parameters that are not available in standard TEVC recordings, such as g_m or E_{rev}.

Our paired-ramp approach may serve cell biologists as a straightforward and real-time method to study the mechanisms of exo-/endocytosis. Electrophysiologists investigating the regulation of ion channels or membrane transporters by hormones and second messengers may use this method as a tool to distinguish direct effects on protein function from indirect effects that are mediated by insertion into or retrieval from the plasma membrane. Finally, the method offers a way to make membrane capacitance one of the parameters that can be exploited for drug screening, now that machines become increasingly available that carry out TEVC and patch-clamp experiments automatically and in high-throughput formats (e.g., Roboocyte, Multichannelsystems, Reutlingen, Germany, or Axon Instruments, Foster City, CA).

We thank Hans-Rainer Polder (NPI Electronic) for discussions and advice on design and mathematical modeling of the model circuit, Werner Baumgartner for help with mathematical modeling, and Wolfgang Schwarz (Max-Planck Institute for Biophysics, Frankfurt, Germany) for critical reading of the manuscript.

This work was supported by a grant from the Deutsche Nierenstiftung to B.M.S. and from the SFB 48 7/C1/A4 to H.K.

REFERENCES

Adrian, R. H., and W. Almers. 1974. Membrane capacity measurements on frog skeletal muscle in media of low ion content. *J. Physiol. (Lond.).* 237:573–605.

Alvarez, d.l. R., P. Zhang, F. T. Naray, G. Fejes-Toth, and C. M. Canessa. 1999. The serum and glucocorticoid kinase sgk increases the abundance of epithelial sodium channels in the plasma membrane of *Xenopus* oocytes. *J. Biol. Chem.* 274:37834–37839.

Angleson, J. K., and W. J. Betz. 1997. Monitoring secretion in real time: capacitance, amperometry and fluorescence compared. *Trends Neurosci.* 20:281–287.

Armstrong, C. M. 1975. Ionic pores, gates, and gating currents. *Q. Rev. Biophys.* 61:644–683.

Awayda, M. S. 2000. Specific and nonspecific effects of protein kinase C on the epithelial Na^+ channel. *J. Gen. Physiol.* 115:559–570.

Baumgartner, W., L. Islas, and F. J. Sigworth. 1999. Two-microelectrode voltage clamp of *Xenopus* oocytes: voltage errors and compensation for local current flow. *Biophys. J.* 77:1980–1991.

Birnir, B., D. D. Loo, and E. M. Wright. 1991. Voltage-clamp studies of the Na^+/glucose cotransporter cloned from rabbit small intestine. *Pflugers Arch.* 418:79–85.

Block, M. L., and W. J. Moody. 1987. Changes in sodium, calcium and potassium currents during early embryonic development of the ascidian *Boltenia villosa*. *J. Physiol. (Lond.).* 393:619–634.

Blumenthal, E. M., and L. K. Kaczmarek. 1992. Modulation by cAMP of a slowly activating potassium channel expressed in *Xenopus* oocytes. *J. Neurosci.* 12:290–296.

Bourinet, E., F. Fournier, P. Lory, P. Charnet, and J. Nargeot. 1992. Protein kinase C regulation of cardiac calcium channels expressed in *Xenopus* oocytes. *Pflugers Arch.* 421:247–255.

Chen, P., and K. D. Gillis. 2000. The noise of membrane capacitance measurements in the whole-cell recording configuration. *Biophys. J.* 79:2162–2170.

Cole, K. S. 1968. Membranes, Ions, and Impulses. University of California Press, Berkeley, CA.

Cole, K. S., and A. L. Hodgkin. 1939. Membrane and protoplasm resistance in the squid giant axon. *J. Gen. Physiol.* 22:671–687.

Curtis, H. J., and K. S. Cole. 1938. Transverse electric impedance of the squid giant axon. *J. Gen. Physiol.* 21:757–765.

Forster, I. C., N. Hernando, J. Biber, and H. Murer. 1998. The voltage dependence of a cloned mammalian renal type II Na^+/P_i cotransporter (NaPi-2). *J. Gen. Physiol.* 112:1–18.

Forster, I. C., M. Traebert, M. Jankowski, G. Stange, J. Biber, and H. Murer. 1999. Protein kinase C activators induce membrane retrieval of type II Na^+-phosphate cotransporters expressed in *Xenopus* oocytes. *J. Physiol. (Lond.).* 517:327–340.

Gentet, L. J., G. J. Stuart, and J. D. Clements. 2000. Direct measurement of specific membrane capacitance in neurons. *Biophys. J.* 79:314–320.

Gillis, K. D. 1995. Techniques for membrane capacitance measurements. *In* Single-Channel Recording. B. Sakmann and E. Neher, editors. Plenum Press, New York. 155–198.

Gillis, K. D. 2000. Admittance-based measurement of membrane capacitance using the EPC-9 patch-clamp amplifier. *Pflugers Arch.* 439: 655–664.

Hirsch, J. R., D. D. Loo, and E. M. Wright. 1996. Regulation of Na^+/glucose cotransporter expression by protein kinases in *Xenopus laevis* oocytes. *J. Biol. Chem.* 271:14740–14746.

Isom, L. L., D. S. Ragsdale, K. S. De Jongh, R. E. Westenbroek, B. F. Reber, T. Scheuer, and W. A. Catterall. 1995. Structure and function of the beta 2 subunit of brain sodium channels, a transmembrane glycoprotein with a CAM motif. *Cell.* 83:433–442.

Johnson, J. W., and S. Thompson. 1989. Measurement of nonuniform current densities and current kinetics in *Aplysia* neurons using a large patch method. *Biophys. J.* 55:299–308.

Kado, R. T. 1993. Membrane area and electrical capacitance. *Methods Enzymol.* 221:273–299.

Keynes, R. D. 1994. The kinetics of voltage gated channels. *Q. Rev. Biophys.* 27:339–434.

Khan, N. A., V. Quemener, and J. P. Moulinoux. 1991. Exogeneous diacylglycerols downregulate the activity of Na^+ -K^+ pump in *Xenopus laevis* oocytes. *Exp. Cell Res.* 194:248–251.

Klamo, E. M., M. E. Drew, S. M. Landfear, and M. P. Kavanaugh. 1996. Kinetics and stoichiometry of a proton/myo-inositol cotransporter. *J. Biol. Chem.* 271:14937–14943.

Kordas, M., Z. Melik, D. Peterc, and R. Zorec. 1989. The voltage-clamp apparatus assisted by a 'current pump'. *J. Neurosci. Methods.* 26: 229–232.

Kusama, T., K. Hatama, K. Saito, Y. Kizawa, and H. Murakami. 2000. Activation of protein kinase C induces internalization of the GABA(C) receptors expressed in *Xenopus* oocytes. *Jpn. J. Physiol.* 50:429–435.

Lindau, M., and E. Neher. 1988. Patch-clamp techniques for time-resolved capacitance measurements in single cells. *Pflugers Arch.* 411:137–146.

Lollike, K., and M. Lindau. 1999. Membrane capacitance techniques to monitor granule exocytosis in neutrophils. *J. Immunol. Methods.* 232: 111–120.

Loo, D. D. F., A. Hazama, S. Supplisson, E. Turk, and E. M. Wright. 1993. Relaxation kinetics of the Na^+ glucose cotransporter. *Proc. Natl. Acad. Sci. U.S.A.* 90:5767–5771.

Loo, D. D., J. R. Hirsch, H. K. Sarkar, and E. M. Wright. 1996. Regulation of the mouse retinal taurine transporter (TAUT) by protein kinases in *Xenopus* oocytes. *FEBS Lett.* 392:250–254.

Mastroberardino, L., B. Spindler, I. Forster, J. Loffing, R. Assandri, A. May, and F. Verrey. 1998. Ras pathway activates epithelial Na^+ channel and decreases its surface expression in *Xenopus* oocytes. *Mol. Biol. Cell.* 9:3417–3427.

McCulloh, D. H., and H. Levitan. 1987. Rabbit oocyte maturation: changes of membrane resistance, capacitance, and the frequency of spontaneous transient depolarizations. *Dev. Biol.* 120:162–169.

Moody, W. J., and M. M. Bosma. 1985. Hormone-induced loss of surface membrane during maturation of starfish oocytes: differential effects on potassium and calcium channels. *Dev. Biol.* 112:396–404.

Moody, W. J., and J. B. Lansman. 1983. Developmental regulation of Ca^{2+} and K^+ currents during hormone-induced maturation of starfish oocytes. *Proc. Natl. Acad. Sci. U.S.A.* 80:3096–3100.

Murray, K. T., S. A. Fahrig, K. K. Deal, S. S. Po, N. N. Hu, D. J. Snyders, M. M. Tamkun, and P. B. Bennett. 1994. Modulation of an inactivating human cardiac K^+ channel by protein kinase C. *Circ. Res.* 75:999–1005.

Nagel, G., C. Volk, T. Friedrich, J. C. Ulzheimer, E. Bamberg, and H. Koepsell. 1997. A reevaluation of substrate specificity of the rat cation transporter rOCT1. *J. Biol. Chem.* 272:31953–31956.

Neher, E. 1971. Two fast transient current components during voltage clamp on snail neurons. *J. Gen. Physiol.* 58:36–53.

Neher, E., and A. Marty. 1982. Discrete changes of cell membrane capacitance observed under conditions of enhanced secretion in bovine adrenal chromaffin cells. *Proc. Natl. Acad. Sci. U.S.A.* 79:6712–6716.

Palti, Y. 1969. Varying potential control voltage clamp of axons. *In* Biophysics and Physiology of Excitable Membranes. 194–205.

Parent, L., S. Supplisson, D. F. Loo, and E. M. Wright. 1992. Electrogenic properties of the cloned Na^+/glucose cotransporter. I. Voltage-clamp studies. *J. Membr. Biol.* 125:49–62.

Peres, A., and G. Bernardini. 1985. The effective membrane capacity of *Xenopus* eggs: its relations with membrane conductance and cortical granule exocytosis. *Pflugers Arch.* 404:266–272.

Peters, K. W., J. Qi, S. C. Watkins, and R. A. Frizzell. 1999. Syntaxin 1A inhibits regulated CFTR trafficking in *Xenopus* oocytes. *Am. J. Physiol.* 277:C174–C180.

Piwon, N., W. Gunther, M. Schwake, M. R. Bosl, and T. J. Jentsch. 2000. CIC-5 Cl^--channel disruption impairs endocytosis in a mouse model for Dent's disease. *Nature.* 408:369–373.

Polder, H.-R., and D. Swandulla. 2001. The use of control theory for the design of voltage clamp systems: a simple and standardized procedure for evaluating system parameters. *J. Neurosci. Methods.* 109:97–109.

Quick, M. W., J. L. Corey, N. Davidson, and H. A. Lester. 1997. Second messengers, trafficking-related proteins, and amino acid residues that contribute to the functional regulation of the rat brain GABA transporter GAT1. *J. Neurosci.* 17:2967–2979.

Rajan, S., E. Wischmeyer, C. Karschin, R. Preisig-Muller, K. H. Grzeschik, J. Daut, A. Karschin, and C. Derst. 2001. THIK-1 and THIK-2, a novel subfamily of tandem pore domain K^+ channels. *J. Biol. Chem.* 276:7302–7311.

Schmalzing, G., H. P. Richter, A. Hansen, W. Schwarz, I. Just, and K. Aktories. 1995. Involvement of the GTP binding protein Rho in constitutive endocytosis in *Xenopus laevis* oocytes. *J. Cell Biol.* 130: 1319–1332.

Sherman, A. J., A. Shrier, and E. Cooper. 1999. Series resistance compensation for whole-cell patch clamp studies using a membrane state estimator. *Biophys. J.* 77:2590–2601.

Stühmer, W. 1998. Electrophysiologic recordings from *Xenopus* oocytes. *Methods Enzymol.* 293:280–300.

Takahashi, A., S. C. Watkins, M. Howard, and R. A. Frizzell. 1996. CFTR-dependent membrane insertion is linked to stimulation of the CFTR chloride conductance. *Am. J. Physiol.* 271:C1887–C1894.

Tong, Y., G. Brandt, M. Li, G. Shapovalov, E. Slimko, A. Karschin, D. Dougherty, and H. Lester. 2001. Tyrosine decaging leads to substantial membrane trafficking during modulation of an inward rectifier potassium channel. *J. Gen. Physiol.* 117:103–118.

Vasilets, L. A., G. Schmalzing, K. Madefessel, W. Haase, and W. Schwarz. 1990. Activation of protein kinase C by phorbol ester induces down-regulation of the Na^+/K^+ -ATPase in oocytes of *Xenopus laevis*. *J. Membr. Biol.* 118:131–142.

Weber, W. M., H. Cuppens, J. J. Cassiman, W. Clauss, and W. Van Driessche. 1999. Capacitance measurements reveal different pathways for the activation of CFTR. *Pflugers Arch.* 438:561–569.

Wright, E. M., J. R. Hirsch, D. D. Loo, and G. A. Zampighi. 1997. Regulation of Na^+/glucose cotransporters. *J. Exp. Biol.* 200:287–293.

Zhang, Y., and O. P. Hamill. 2000. On the discrepancy between whole-cell and membrane patch mechanosensitivity in *Xenopus* oocytes. *J. Physiol. (Lond.).* 523:101–115.

Zhu, S. J., M. P. Kavanaugh, M. S. Sonders, S. G. Amara, and N. R. Zahniser. 1997. Activation of protein kinase C inhibits uptake, currents and binding associated with the human dopamine transporter expressed in *Xenopus* oocytes. *J. Pharmacol. Exp. Ther.* 282:1358–1365.